PLANT SCIENCE

Ground tissue circuitry regulates organ complexity in maize and *Setaria*

Carlos Ortiz-Ramírez[1,2], Bruno Guillotin[1]†, Xiaosa Xu[3]†, Ramin Rahni[1]†, Sanqiang Zhang[1], Zhe Yan[4]‡, Poliana Coqueiro Dias Araujo[1]§, Edgar Demesa-Arevalo[3], Laura Lee[1], Joyce Van Eck[5,6], Thomas R. Gingeras[3], David Jackson[3], Kimberly L. Gallagher[4], Kenneth D. Birnbaum[1]*

Most plant roots have multiple cortex layers that make up the bulk of the organ and play key roles in physiology, such as flood tolerance and symbiosis. However, little is known about the formation of cortical layers outside of the highly reduced anatomy of *Arabidopsis*. Here, we used single-cell RNA sequencing to rapidly generate a cell-resolution map of the maize root, revealing an alternative configuration of the tissue formative transcription factor SHORT-ROOT (SHR) adjacent to an expanded cortex. We show that maize SHR protein is hypermobile, moving at least eight cell layers into the cortex. Higher-order *SHR* mutants in both maize and *Setaria* have reduced numbers of cortical layers, showing that the *SHR* pathway controls expansion of cortical tissue to elaborate anatomical complexity.

Roots are radially symmetrical organs composed of three fundamental tissue types: the epidermis on the outside, the ground tissue at the middle, and a core of vascular elements plus pericycle that lie in a central cylinder known as the stele (*1*). The ground tissue is further divided into two different cell types, the endodermis and cortex, which are arranged as concentric layers around the stele. Variations in ground tissue patterning, particularly the number of cortex cell layers, are common across species and represent one of the defining features giving rise to interspecies root morphological diversity (*1*). This diversity allows plants to cope with biotic and abiotic stress and adapt to challenging environments. For example, maize cortex plays a role in drought and flood tolerance and hosts colonization of beneficial mycorrhizal associations that reduce stress and improve nutrient uptake (*2*–*5*). Therefore, an ongoing question in root biology is how tissue patterning is adjusted to produce divergent root morphologies, and what alterations in the genetic networks control developmental differences among species.

A current limitation is that knowledge of radial patterning mechanisms in roots comes largely from the study of *Arabidopsis*, which possesses a simple root anatomy. In *Arabidopsis*, only two ground tissue layers develop in primary development—one endodermal and one cortical—that originate from an asymmetric cell division at or near the initials or stem cells (*6*). This division is controlled by the *SHORT-ROOT* (*SHR*)–*SCARECROW* (*SCR*) genetic pathway (*7*, *8*). Mutants in either transcription factor develop a monolayered ground tissue. In addition, SHR mutants lack an endodermis, giving *SHR* a role in both tissue formation and cell identity (*9*).

SHR functions as a mobile signal whose protein travels from the stele, where the gene is transcribed, into the surrounding endodermis, where it induces the expression of the downstream transcription factor *SCR* (*8*). The pathway then triggers the division that generates the cortex and endodermis layers (*9*). In maize, the *SHR-SCR* pathway has been implicated with a role in leaf anatomy (*10*–*13*). Movement of SHR from the stele further out into the cortex could potentially cause extra cell divisions, giving rise to multiple cortex layers (*12*). Supporting this idea, the SHR-SCR pathway was recently implicated in cortical cell division during nodule formation in the dicot *Medicago* (*14*). However, the role of *SHR* in the expansion of cortical layer number in maize, a monocot, is not known.

Dye penetrance labeling for rapid tissue profiling

We sought to produce a high-resolution spatial and temporal map of gene expression in a complex root that could provide clues to the genetic networks controlling morphological diversity in patterning. Therefore, we generated cell type–specific gene expression profiles using high-throughput single-cell RNA sequencing (scRNAseq) to profile maize roots. Maize is a valuable model for comparative studies because its roots develop multilayered cortical tissues (8 to 9 cortex cell layers) within the root meristem and it is amenable to protoplast generation, an essential step in plant scRNAseq (*15*). However, a challenge of scRNAseq studies in species for which genomic resources are limited is the correct identification of cell types. The use of homologs of *Arabidopsis* markers obtained by high-throughput cell sorting did not provide a clear identification of morphologically homologous cell types in maize. This is likely because gene orthology is not always apparent and localization over such broad evolutionary distance is not well conserved.

To overcome this problem, we first took advantage of the concentric arrangement of tissues in roots to develop a technique to fluorescently mark cell layers by dye penetrance labeling (DPL). In brief, a highly penetrant dye (Syto 40 blue) stains the entire root with low but detectable staining in stele, whereas a weakly penetrant dye (Syto 81 green) stains the outer tissue layers strongly, with a gradual drop in signal intensity toward the inner tissues (Fig. 1A). This dual labeling was reproducible across roots and batches and had a negligible effect on transcription (fig. S1). The approach allowed us to enrich for different concentric tissue layers using blue/green ratios in fluorescence-activated cell sorting (FACS). We calibrated dye ratio to radial position by using DPL on a line expressing a fluorescent protein driven by the *SCR* promoter (*ZmSCR1*::*RFP*; Fig. 1, A and B), which expresses in the endodermis. Red fluorescent protein (RFP)–positive cells were used to calibrate a reference dye ratio for this middle layer, allowing demarcation of inner and outer tissues (Fig. 1, B and C, and fig. S2A). We dissected seminal root tips (5 mm and, in one subset, 5 to 8 mm from the root tip) and then rapidly enzymatically digested their cell walls, sorting cells belonging to different tissue layers using their specific dye ratio. We also generated a set of whole meristem protoplasts versus intact root controls to filter out any effects of cell wall digestion. Digested and undigested controls clustered closely together, and replicate samples yielded consistent profiles (fig. S2, B to D). In addition, we obtained expression profiles of the root cap by dissection and quiescent center (QC), using FACS on a stable QC marker line, *ZmWOX5*::RFP (fig. S2E). To validate the entire dataset, we compared the six tissue expression profiles to known markers and to a previous study that used mechanical separation of inner versus outer layers (*16*), finding 80% agreement or higher (Fig. 1, D and E). We also used a panel of conserved and well-characterized markers to validate sorted-cell profiles, showing close agreement (fig. S3 and table S1). In this manner, we developed a set of at least 170 markers for each radially arranged tissue (table S2).

[1]Center for Genomics and Systems Biology, Department of Biology, New York University, New York, NY 10003, USA. [2]UGA Laboratorio Nacional de Genómica para la Biodiversidad, CINVESTAV Irapuato, Guanajuato 36821, México. [3]Cold Spring Harbor Laboratory, Cold Spring Harbor, NY 11724, USA. [4]School of Arts and Sciences, University of Pennsylvania, Philadelphia, PA 1904, USA. [5]Boyce Thompson Institute, Ithaca, NY 14853, USA. [6]Plant Breeding and Genetics Section, School of Integrative Plant Science, Cornell University, Ithaca, NY 14853, USA.
*Corresponding author. Email: ken.birnbaum@nyu.edu
†These authors contributed equally to this work.
‡Present address: The National Key Facility for Crop Gene Resources and Genetic Improvement (NFCRI)/Key Lab of Germplasm Utilization (MOA), Institute of Crop Sciences, Chinese Academy of Agricultural Sciences, Beijing 100081, China.
§Present address: Department of Agronomic and Forest Sciences, Universidade Federal Rural do Semi-Árido, RN, Brazil.

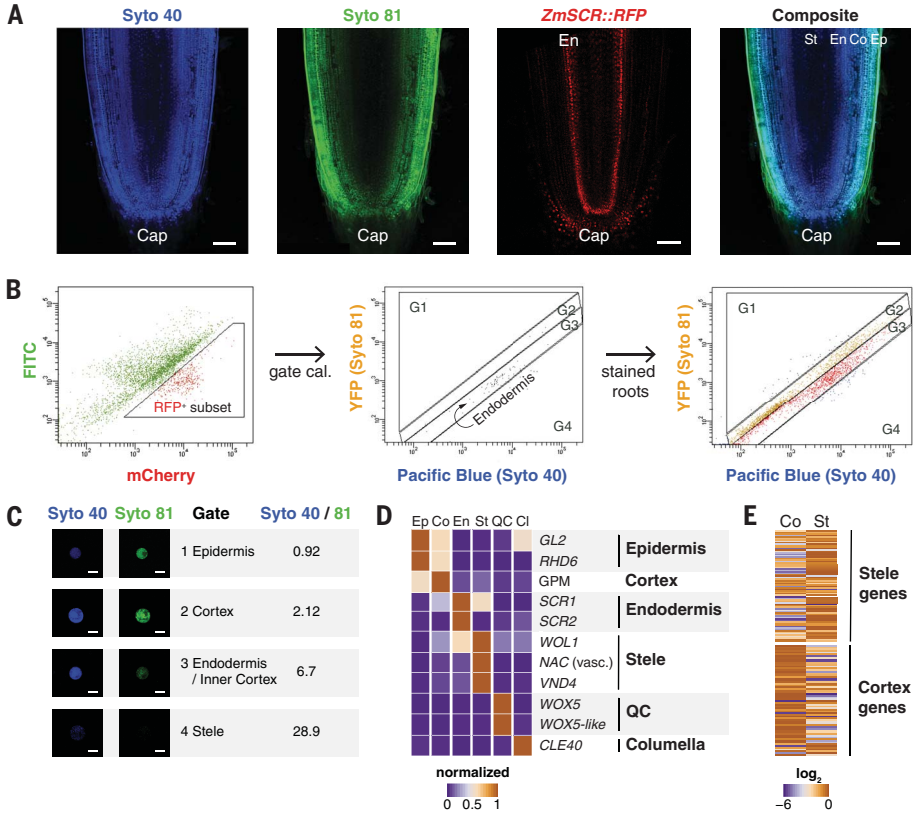

Fig. 1. Dye penetrance labeling (DPL) and tissue transcriptome analysis in maize. (**A**) Representative images of a deeply penetrating dye (Syto 40), a superficially penetrating dye (Syto 81), the *ZmSCR*::RFP marking endodermis, and a composite image of Syto 40 and Syto 81 staining. (**B**) Cell sorting gating strategy, showing the *ZmSCR*::RFP population (left), backgated onto a YFP versus Pacific blue plot with RFP positive (middle), and (right) the gated boundaries for endodermal, outside of endodermis (G1, G2), and inside of endodermis (G4). FITC, fluorescein-5-isothiocyanate. (**C**) Validation of ratiometric cell sorting strategy by collecting sorted cells from gates and quantifying fluorescence from microscopy images. (**D**) Validation of sorted cell RNA-seq profiles by analysis of known markers. (**E**) Global validation comparing sorted cells versus mechanically dissected stele and cortex tissues, with heat map showing expression in sorted cortex versus stele gates, categorized by previously determined stele and cortex markers. Scale bars, 100 μm (A) and 15 μm (C).

A single-cell map of the maize root

To generate a single-cell resolution map of the maize root meristem, we then dissected seminal root tips from 7-day-old wild-type B73 maize seedlings and enzymatically digested their cell walls, as above. We then used the cells to prepare single-cell cDNA libraries using the 10x Genomics Chromium platform. A total of 14,755 high-quality cells were sequenced in three different batches with a mean of 31,105 unique molecular indices per cell and 5683 detected genes per cell (fig. S4). A total of 21 cell clusters were defined and visualized in two dimensions in Seurat using the uniform manifold approximation and projection (UMAP) method (*17*). To quantify cell identity and classify clusters using the DPL markers, we applied the Index of Cell Identity (ICI) algorithm (*18*), which generates a cell identity score based on the mean expression of a predefined marker gene set, in this case, from FACS-isolated tissues (Fig. 2A and figs. S5 and S6). Overall, the technique allowed us to identify all the UMAP clusters, providing a detailed spatial map of transcripts in specific cell types of the maize root (Fig. 2B).

The high-resolution cellular map of the meristem showed multiple cell type subclusters within the stele and cortex, suggesting cellular specialization within the latter tissue's multiple layers. However, because root cells differentiate as they transition away from the root tip, the possibility remained that some subclusters represented different maturation states of an individual cell type. To distinguish subclusters formed by distinct identity rather than differentiation state, we further generated a set of cell maturation marker transcripts by dissecting 16 longitudinal root slices that together comprised the meristematic, transition, and elongation zones, and we subjected the samples to RNAseq analysis (Fig. 2C). Using K-means clustering, we identified three main expression programs: early meristematic (high expression in the meristem and gradual decrease toward the transition zone), transition zone (specific to the mid-maturation point), and posttransition (low expression in the meristematic zone and gradual increase toward the elongation zone). We then generated a cellular differentiation score to label the maturation status of each cell, resolving developmental trajectories of cells in our high-resolution map of cell identities (Fig. 2D).

High-resolution profiling reveals cortical complexity

In a few cases, the state of cell maturation is indeed the main factor influencing grouping of cells into subclusters. For example, five clusters (8, 11, 12, 14, and 16) had the same identity but a different maturation state compared with adjacent clusters. However, the majority of subclusters were composed of cells with a wide range of differentiation states, showing that the grouping in most cases represented distinct cell identities. Although two cortex subclusters appeared to be a precursor state of mature cortex (clusters 8 and 14), our analysis confirmed the existence of at least four distinct cortex subtypes (clusters 1, 2, 13, and 19; Fig. 2B). Furthermore, using the receiver operating characteristic analysis in Seurat, which identified 2436 differentially expressed genes (DEGs) across all clusters, we found 471 transcripts that mark some subset of the four different cortical subtypes (Fig. 2E and table S3). Thus, we provide quantitative evidence for the subspecialization of cortex that underlies expansion of root complexity, yielding strong evidence for cortical cell diversification.

One question that follows is what signaling mechanisms allow maize to form the extra layers that permit cortex subspecialization. We observed that a short list of functional markers with a role in patterning or cell identity in *Arabidopsis* had conserved localization in homologous tissues in maize (e.g., *CO2*, cortex; *MYB46*, xylem; *RHD6*, epidermis; and *LBD29*, stele) (Fig. 2E). However, our scRNAseq data showed that expression of the core patterning gene *SHR* was specific to the endodermis and not to the stele (Fig. 2E), where the *Arabidopsis* ortholog is expressed (*9*). All three maize paralogs of *SHR* (designated *ZmSHR1*, *ZmSHR2*, and *ZmSHR2-h*) showed the same endodermal enrichment in the profiles generated by DPL and single-cell analysis (Fig. 3, A and B). We speculated that the expression of this mobile, division-inducing transcription factor adjacent to the cortex could be related to a role in the expansion of that tissue.

Mobile SHR regulates cortical complexity in maize and *Setaria*

To confirm SHR transcript localization, we performed in situ hybridization on all three *SHR*

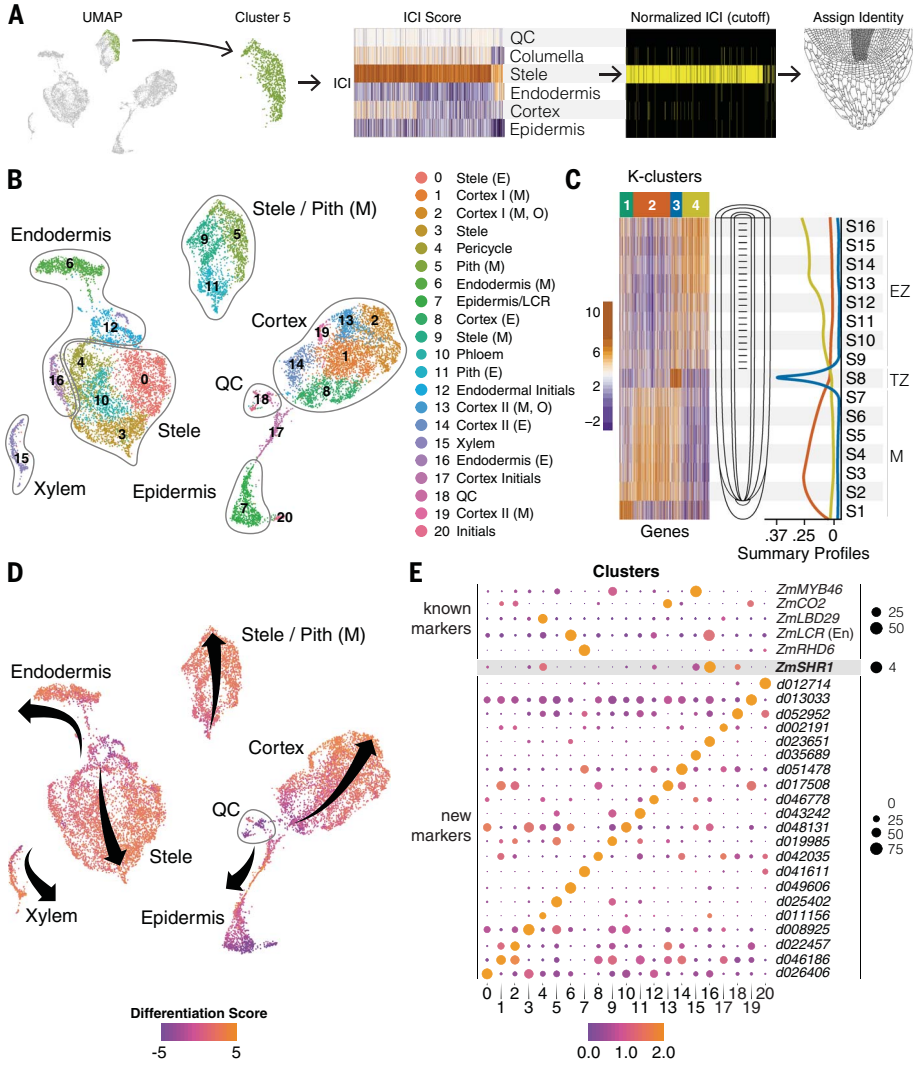

Fig. 2. Single-cell RNA-seq spatial and temporal transcriptome maps of the maize meristem. (**A**) The ICI method of diagnosing cell identity of UMAP clusters using known markers and randomization testing (e.g., cluster 5). (**B**) Cluster identities as determined by ICI and cell-type specific markers (E, early; M, mature; O, outer; Pith, pith parenchyma). (**C**) Heat map of highly variant genes along a longitudinal axis of the root meristem. Developmental patterns show transcripts and markers that peak in the early meristem (M), transition zone (TZ), and elongation zone (EZ). (**D**) Trajectories of developmental "pseudo-time" in each cell cluster mapped onto the same UMAP depicted in (B), where a differentiation score is calculated as a $\log_2$ ratio of all EZ/M markers identified in (C). Arrow origins for each cluster represent cells in the meristem near the stem cells progressing to more proximal cells near the arrowheads. (**E**) Select known (top) and new markers (bottom) for each cluster. Size of spot represents percent of cells in cluster expressing the marker, and color represents their relative expression level in those cells.

mRNAs, confirming their localization in the endodermis (Fig. 3, C to E, and fig. S7, A to I). A 1.4-kb upstream and downstream transcriptional reporter for *ZmSHR2* also showed signal in the root endodermis, in agreement with our dye-sorted and single-cell profiles (Fig. 3D). No signal was found in the stele, confirming that *SHR2* transcript localizes to different cell types in maize compared with *Arabidopsis*. Consistently, the *ZmSHR* endodermal domain in the root is reminiscent of *ZmSHR* expression in the shoot bundle sheath (*19*, *20*), which is in an analogous position to root endodermis. In addition, expression of *SHR* orthologs was shown to localize to the endodermis in date palm (*21*).

Given evidence that rice SHR proteins are hypermobile when expressed heterologously in *Arabidopsis* (*8*), we assessed whether maize SHR protein could move from the endodermis, where its mRNA is expressed, into the adjacent cortex. For this purpose, we made a natively expressed protein reporter of ZmSHR1 fused to yellow fluorescent protein (*ZmSHR1*::*SHR1*-YFP). Indeed, compared to endodermal localization of the *ZmSHR1* transcript, the maize SHR1 protein reporter was present in the cortex (Fig. 3F). Moreover, SHR1-YFP signal was not restricted to the adjacent tissue layer as in *Arabidopsis* but was observed in all cortex layers, suggesting that the endogenous maize SHR1 protein moves through at least eight cortex layers (Fig. 3F and fig. S7E). In addition, the ZmSHR1 protein also appeared to be hypermobile when expressed in the endodermis of *Arabidopsis* (fig. S8, A and B). Whether additional SHR paralogs are mobile is an open question.

SHR's role in promoting division in *Arabidopsis* works through direct interaction with SCR (*22*). Therefore, we also generated maize *SCR* reporter lines to determine colocalization with *SHR*. Both in situ localization and a promoter RFP reporter revealed a strong signal in the root endodermis, as shown previously (*23*) and similar to its localization in *Arabidopsis* (Fig. 3G and fig. S7, F to I). In addition, we observed low-level cortical expression of *SCR1* in both the scRNAseq data and high-sensitivity confocal imaging (e.g., fig. S7G). However, natively expressed ZmSCR-GFP protein fusions showed a signal in the stele, suggesting that SCR protein in maize moves from cell to cell in the opposite direction from that of SHR (Fig. 3H and fig. S8C). Our results show that SHR and SCR colocalize in the endodermis and possibly in the cortex. A SCR translational reporter in a second monocot, *Setaria viridis* (*Setaria*), showed the same localization in the stele, further corroborating the divergent localization of SCR protein in monocots (fig. S9, A and B).

The model that implicates SHR in cortical expansion posits that increased outward movement of the protein could trigger periclinal cell divisions giving rise to extra ground tissue layers (*12*). To test the model, we targeted the three different maize *SHR* paralogs to generate loss-of-function mutants in maize using CRISPR-Cas9 (fig. S10, A and B). We recovered mutants in two of the genes (*ZmSHR2* and *ZmSHR2-h*), including the most highly expressed paralog, *ZmSHR2*. Single mutants in *Zmshr2* or *Zmshr2-h* had no difference in their root anatomy compared to wild-type siblings. However, *Zmshr2/2-h* double mutants had a significant reduction in the number of cortical layers, with most roots having seven layers compared with eight or nine layers in wild type (Fig. 4, A to D). Mutants in the single *SHR* gene in *Arabidopsis* lack an endodermal layer. However, staining for suberin and morphological analysis showed that *Zmshr2/2-h* roots still developed an endodermis (fig. S11). We posit that the remaining functional *ZmSHR1* gene in the *Zmshr2/2-h* background may still enable specification of endodermal identity. Alternatively, *ZmSCR1* (and *ZmSCR2*) may be the primary factors in the specification of the maize endodermis (*13*). Overall, our results suggest

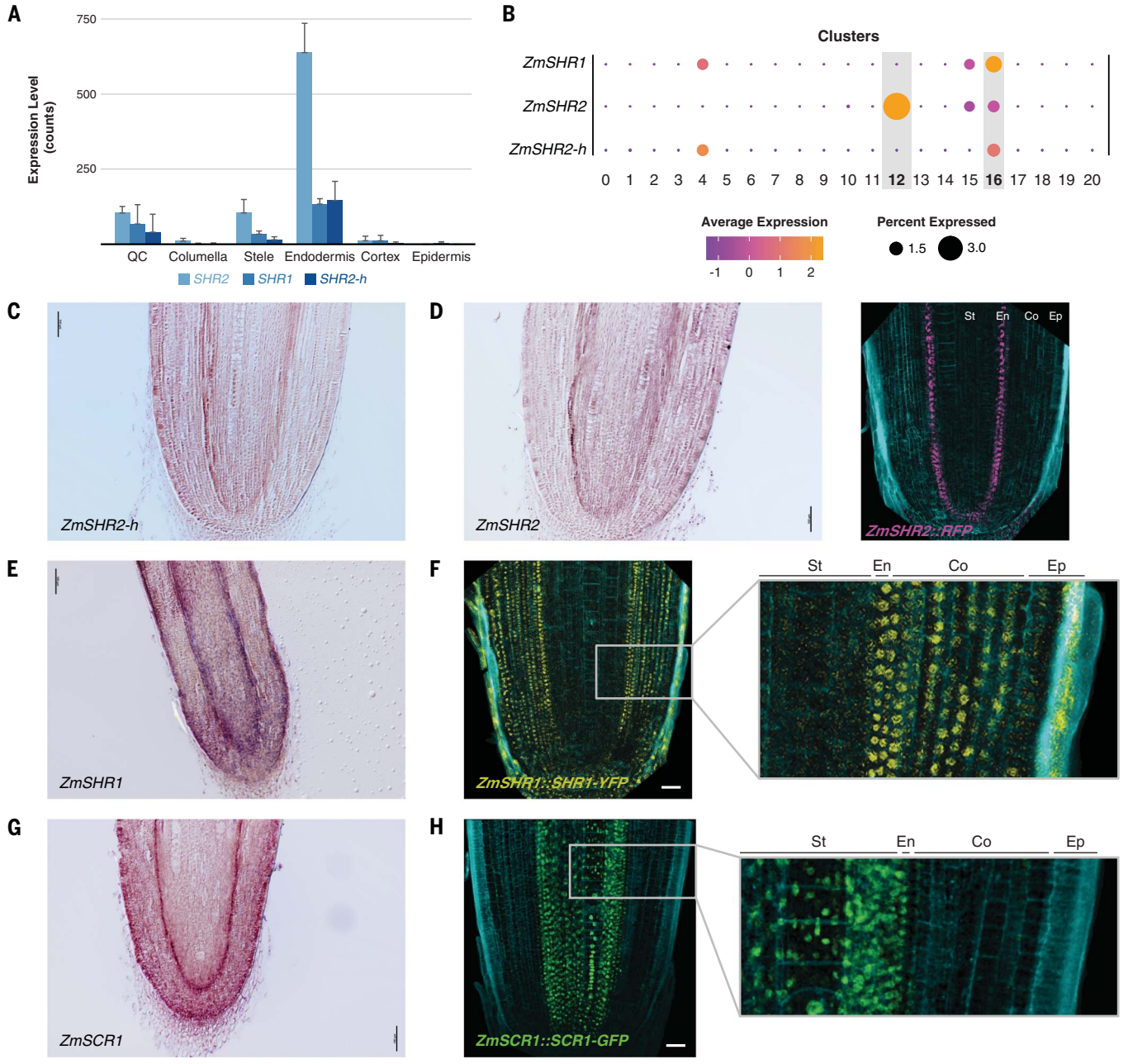

Fig. 3. SHR and SCR expression in maize endodermis and differences between transcriptional and translational reporters. (**A**) Expression of the three *ZmSHR* paralogs (*SHR1,2,2-h*) from sorted cells. Error bars are SDs. (**B**) Dot plots representing scRNAseq analysis showing expression of *ZmSHR* paralogs in endodermis and, at a low level, stele. (**C**) *ZmSHR2-h* in situ hybridization showing endodermal expression. (**D**) *ZmSHR2* in situ hybridization and transcriptional RFP reporter. (**E**) In situ hybridization of *ZmSHR1*. (**F**) Translational YFP reporter for *Zm*SHR1 with inset showing protein in cortex layers. (**G**) In situ hybridization of *ZmSCR1*. (**H**) Translational reporter SCR1-GFP reporter showing protein in the stele. Scale bars, 50 μm [(F) and (H)] and 100 μm [(C), (D), (E), and (G)]. Cyan in confocal images [(D), (F), (H)] is autofluorescence at an excitation wavelength of 405 nm.

that *SHR* function in maize is necessary for the full expansion of cortical identity.

We sought to validate the monocot *SHR* mutant phenotype with a more severe loss of function by testing its role in *S. viridis*, a close relative of maize. In *Setaria*, we were able to generate loss-of-function mutants in the two *SHR* orthologs using CRISPR-Cas9 (fig. S12, A and B). One *Setaria SHR* mutant, *Svshr2*, showed a slight reduction in cortical layers, and a single mutant in the second, *Svshr1*, showed no phenotype. However, double mutants showed a marked reduction in the number of ground tissue layers, resulting in one to two layers compared to four to five layers in wild-type siblings (Fig. 4, E to H). These results corroborate the role of *SHR* in controlling the expansion of cortical layers in two monocots.

The extra cortical divisions mediated by SHR could function through direct interaction with SCR by mediating successive divisions of the endodermis near the stem cell niche. Alternatively, SHR hypermobility could lead to divisions directly in the cortical layers possibly interacting with low levels of SCR or another protein. At present, we cannot distinguish between these two models.

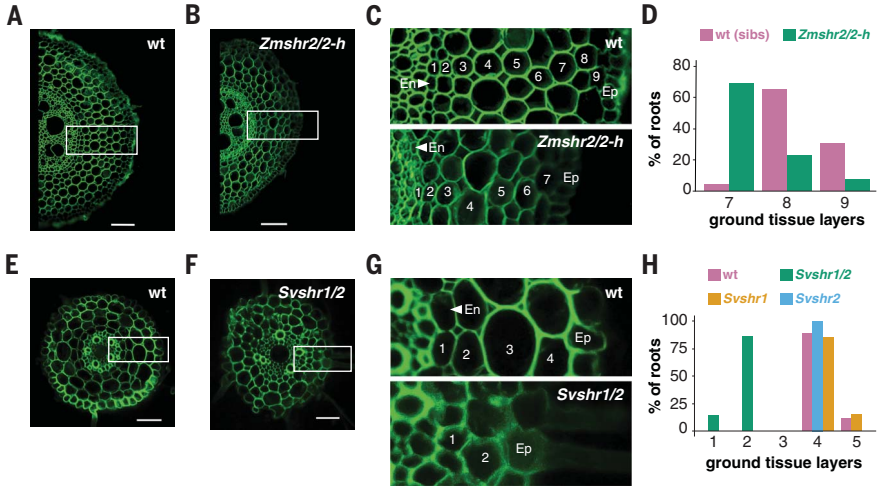

Fig. 4. Cortical cell layer analysis in wild-type and *shr* mutants in monocots. (**A** and **B**) Representative maize root cross sections of wild-type (sibs) (A) versus *Zmshr2/2-h* double homozygous mutant (B). (**C**) Enlarged regions from boxes in (A) and (B) showing endodermal (Ed), cortical (numbered), and epidermal (Ep) layers of wild-type (top) and *Zmshr2/2-h* mutant (bottom). (**D**) Quantification of the cortical cell layers in wild-type and heterozygous sibs (sample size (*n*) = 23) versus *Zmshr2/2-h* mutant (*n* = 13, $p < 0.001$, Mann-Whitney rank test). (**E** and **F**) Representative cross sections of *Setaria* wild type (E) and *Svshr1/2* mutants (F). (**G**) Enlarged regions from dashed boxes in (E) and (F) showing endodermal (Ed), cortical (numbered), and epidermal (Ep) layers of wild type (top) and *Svshr1/2* mutant (bottom). (**H**) Quantification of cortical layers in *Setaria* wild type (*n* = 9), *Svshr1* single (*n* = 7), *Svshr2* single (*n* = 6), and *Svshr1/2* double mutants (*n* =7, $p < 0.001$, Tukey test after one-way analysis of variance on all genotypes,). Scale bars, 100 μm [(A) and (C)] and 50 μm [(E) and (F)]. Green is autofluorescence at an excitation wavelength of 405 nm and emission wavelengths of 510 to 535 nm.

The results show that SHR has a role in monocots in controlling the expansion of cortex, which sets up many traits for environmental acclimation. This illustrates how subtle divergence of a conserved developmental regulator can mediate anatomical complexity that has given rise to specialized functions. Related to the complexity of the root, we identify four distinct cortical cellular subtypes in our bioinformatic analysis, although further work is needed to verify their spatial relationship. Finally, the results show that rapid transcriptome mapping using single-cell dissection can provide insights into the mechanisms that mediate anatomical diversity. The use of dye labeling to generate a scaffold locational map together with scRNAseq provides a maize root tissue map that can be used as a reference in maize and related plants.

REFERENCES AND NOTES

1. K. Esau, *Anatomy of Seed Plants* (Wiley, ed. 2, 1977).
2. M. Kaldorf, A. J. Kuhn, W. H. Schröder, U. Hildebrandt, H. Bothe, *J. Plant Physiol.* **154**, 718–728 (1999).
3. F. Liu *et al.*, *Plant Cell Physiol.* **59**, 1683–1694 (2018).
4. J. Zhu, K. M. Brown, J. P. Lynch, *Plant Cell Environ.* **33**, 740–749 (2010).
5. A. H. Gunawardena, D. M. Pearce, M. B. Jackson, C. R. Hawes, D. E. Evans, *Planta* **212**, 205–214 (2001).
6. L. Dolan *et al.*, *Development* **119**, 71–84 (1993).
7. P. N. Benfey *et al.*, *Development* **119**, 57–70 (1993).
8. K. Nakajima, G. Sena, T. Nawy, P. N. Benfey, *Nature* **413**, 307–311 (2001).
9. Y. Helariutta *et al.*, *Cell* **101**, 555–567 (2000).
10. T. L. Slewinski *et al.*, *Mol. Plant* **7**, 1388–1392 (2014).
11. T. L. Slewinski, A. A. Anderson, C. Zhang, R. Turgeon, *Plant Cell Physiol.* **53**, 2030–2037 (2012).
12. S. Wu *et al.*, *Proc. Natl. Acad. Sci. U.S.A.* **111**, 16184–16189 (2014).
13. T. E. Hughes, O. V. Sedelnikova, H. Wu, P. W. Becraft, J. A. Langdale, *Development* **146**, dev.177543 (2019).
14. W. Dong *et al.*, *Nature* **589**, 586–590 (2021).
15. A. Senn, P.-E. Pilet, *Z. Pflanzenphysiol.* **100**, 299–310 (1980).
16. N. Opitz *et al.*, *J. Exp. Bot.* **67**, 1095–1107 (2016).
17. T. Stuart *et al.*, *Cell* **177**, 1888-1902 e1821 (2019).
18. I. Efroni, P. L. Ip, T. Nawy, A. Mello, K. D. Birnbaum, *Genome Biol.* **16**, 9 (2015).
19. Y. M. Chang *et al.*, *Plant Physiol.* **160**, 165–177 (2012).
20. X. Xu *et al.*, *Dev. Cell* **56**, 557–568.e6 (2021).
21. T. T. Xiao *et al.*, *Plant Cell* **31**, 1751–1766 (2019).
22. H. Cui *et al.*, *Science* **316**, 421–425 (2007).
23. J. Lim *et al.*, *Plant Cell* **12**, 1307–1318 (2000).

ACKNOWLEDGMENTS

Funding: K.D.B and D.J. are supported by NSF grant IOS-1934388. K.D.B, D.J., and T.R.G. were supported by NSF grant IOS 1445025. K.D.B. is funded by NIH grant R35GM136362. D.J. is funded by NSF IOS-1930101. K.L.G. is funded by NSF PGRP-23020. B.G. is funded by the Human Frontier Science Program Organization grant: LT - 000972/2018. **Author contributions:** C.O.-R., B.G., S.Z., and L.L. performed all transcriptomic experiments and expression analysis. C.O.R. performed mutant analysis. C.O.R. and K.D.B. designed the experiments and wrote the manuscript. C.O.R., K.D.B., D.J., T.R.G., and K.L.G. conceived the project and guided the experiments. X.X. performed in situ hybridizations. P.C.D.A. and S.Z. assisted in mutant analysis and marker analysis. R.R. designed and carried out microscopy protocols and designed graphic layouts. E.D.-A. and X.X. generated transcriptional reporters in maize. C.O.R., Z.Y., and J.V.E generated CRISPR-Cas9 knockouts and translational reporters in maize and *Setaria* and generated the *Setaria* mutants. **Competing interests:** The authors declare no competing interests. **Data materials and availability:** All data are included in the main paper or the supplementary materials or are deposited at the Gene Expression Omnibus website (https://www.ncbi.nlm.nih.gov/geo/) under the SuperSeries accession number GSE172302. *pZmWOX5::RFP*, *pZmSCR1::RFP*, and *pZmSHR2::RFP* reporter lines are available from D.J. under a material transfer agreement with Cold Harbor Spring Laboratory.

SUPPLEMENTARY MATERIALS

science.org/doi/10.1126/science.abj2327
Materials and Methods
Figs. S1 to S13
Tables S1 to S3
References (*24–30*)
MDAR Reproducibility Checklist

View/request a protocol for this paper from *Bio-protocol*.

28 April 2021; accepted 13 October 2021
10.1126/science.abj2327